Available online at www.sciencedirect.com
SCIENCE DIRECT®
Applied Surface Science 252 (2006) 3342–3351
applied surface science
www.elsevier.com/locate/apsusc

Characterization of a SiC/SiC composite by X-ray diffraction, atomic force microscopy and positron spectroscopies

G. Brauer [a,*], W. Anwand [a], F. Eichhorn [a], W. Skorupa [a], C. Hofer [b], C. Teichert [b], J. Kuriplach [c], J. Cizek [c], I. Prochazka [c], P.G. Coleman [d], T. Nozawa [e], A. Kohyama [f]

[a] *Institut für Ionenstrahlphysik und Materialforschung, Forschungszentrum Rossendorf e.V., PF 510119, D-01314 Dresden, Germany*
[b] *Institut für Physik, Montanuniversität Leoben, Franz Josef Str. 18, A-8700 Leoben, Austria*
[c] *Department of Low Temperature Physics, Faculty of Mathematics and Physics, Charles University, V Holesovickach 2, CZ-180 00 Prague, Czech Republic*
[d] *Department of Physics, University of Bath, Bath BA2 7 AY, UK*
[e] *Metals and Ceramics Division, Oak Ridge National Laboratory, P.O. Box 2008, MS6151, Oak Ridge, TN 37831-6151, USA*
[f] *Institute of Advanced Energy, Kyoto University, Gokasho, Uji, Kyoto 611-0011, Japan*

Available online 21 October 2005

Abstract

A SiC/SiC composite is characterized by X-ray diffraction, atomic force microscopy and various positron spectroscopies (slow positron implantation, positron lifetime and re-emission). It is found that besides its main constituent 3C–SiC the composite still must contain some graphite. In order to better interpret the experimental findings of the composite, a pyrolytic graphite sample was also investigated by slow positron implantation and positron lifetime spectroscopies. In addition, theoretical calculations of positron properties of graphite are presented.

Keywords: SiC/SiC composite; Graphite; X-ray diffraction; Atomic force microscopy; Slow positron spectroscopy; Positron lifetime; Positron affinity; Positron re-emission

1. Introduction

Silicon carbide (SiC) fibre-reinforced SiC matrix composite materials (SiC/SiC) are considered to be the attractive candidates as materials for advanced energy systems, such as high performance combustion

* Corresponding author. Tel.: +49 351 2602117; fax: +49 351 2603285.
E-mail address: g.brauer@fz-rossendorf.de (G. Brauer).

0169-4332/$ – see front matter © 2005 Elsevier B.V. All rights reserved.
doi:10.1016/j.apsusc.2005.08.096

systems, fuel-flexible gasification systems, fuel cell/turbine hybrid systems, nuclear fusion reactors and high temperature gas-cooled fission reactors [1]. Recently, a review of state-of-the-art achievements in production and application of SiC/SiC composites was published [2].

It has long been known that SiC is a polytypic substance. But the formation of a phase diagram is very difficult, for annealing is slow; different forms may grow under almost identical conditions, and even small quantities of impurities may have significant effects. From previous studies, it was found that especially the cubic form grows under conditions where one of the hexagonal polytypes is more stable. First explanations of this fact were given in terms of a stacking reversal at a surface and bulk polytype energies [3]. A later extension of this idea was based on a distinction between the two different (0 0 0 1) surfaces and application of bulk-derived parameters at a surface [4].

The positron affinity is a fundamental bulk quantity of a solid, which does not depend on the surface orientation of a crystalline sample, and it has already been calculated for 3C–SiC and 6H–SiC polytypes [5]. At the same time, an experimental estimation of the electron work function of 6H–SiC, combined with independent positron work-function measurements on the same specimen, allowed the evaluation of the positron affinity and its comparison with the theoretical value. This comparison has prompted suggestions for improvements in the theoretical calculations to be confirmed by future work.

The observation of copious positron re-emission from crystalline 6H–SiC, due to a negative positron work function and with no pre-treatment and without the need for ultra-high vacuum conditions, suggests this material may form the basis of an important new moderator for the production of monoenergetic positron beams [6].

Furthermore, SiC in monocrystalline, hexagonal polytype form is a very interesting material for a wide class of novel applications in electronics [7]. An essential step in most of the state-of-the-art technologies is ion implantation, which is used to confine the lateral dimensions of an area of a crystal wafer, or film on a substrate, to be modified. Therefore, the detection and characterization of lattice defects is an essential need and challenge for materials science.

Positron annihilation spectroscopy (PAS) is generally suited to detect, distinguish, and eventually identify open volume defects in solids, including semiconductors [8]. Slow positron implantation spectroscopy (SPIS), based on the generation, implantation and subsequent annihilation of monoenergetic positrons in a sample, is well suited to study depth dependent vacancy-type damage in silicon carbide [9]. In addition, atomic force microscopy (AFM) [10,11] is a suitable method to investigate the surface morphology of a sample.

Recently, systematic SPIS and AFM studies of various 6H–SiC samples, differing in their conductivity type, crystal quality, ion implantation conditions and annealing, were conducted in order to see if and how these parameters may influence the formation of continuous long furrows (undulations) running in one direction across the wafer surface [12]. It was found that the observed changes in surface morphology are primarily the result of thermal activation during annealing and thus occur independent of conductivity type, crystal quality and ion implantation. Moreover, it was observed that the changes in surface morphology have no influence on the defect depth profiling by SPIS.

Based on the experience in studying basic properties and near surface defects in single-crystalline 6H–SiC [5,6,9,12], it is challenging to investigate a SiC/SiC composite made from nano-crystalline 3C–SiC. Following the specification of the preparation conditions of such a composite, results of various experimental investigations, namely X-ray diffraction (XRD), AFM, SPIS and the re-emission of positrons, will be presented and discussed. In addition, some experimental and theoretical results for graphite are presented to complement these discussions. Conclusions are drawn at the end of the paper.

2. Preparation of a SiC/SiC composite

The preparation of a sample having the dimensions 10 mm × 10 mm × 1 mm was performed by the nano-infiltration transient eutectic phase sintering (NITE) process [13] in four steps as follows: (1) selection of a 3C–SiC nano-powder (∼30 nm diameter; Marketech International Inc., Port Townsend/WA, USA, as determined by XRD and transmission

electron microscopy (TEM)) and sintering additives ($Al_2O_3 + Y_2O_3$ = 12 wt.% (Al_2O_3:Y_2O_3 = 60:40) and SiO_2 = 3 wt.%); (2) preparation of a matrix slurry (3C–SiC nano-powder and sintering additives in ethylene solution); (3) infiltration of matrix slurry into the fabrics (fibre: ~500 nm near-stoichiometric SiC continuous Tyranno^{TM}-SA Grade-3, Ube Industries Ltd., Ube, Japan, covered with pyrolytic carbon; architecture: unidirectional cross-plies; fibre volume fraction: 40%); (4) sintering (1.780 °C, Ar atmosphere, 20 MPA pressure, 1 h).

3. Results and discussion

3.1. X-ray diffraction

A standard phase analysis was performed by XRD in Bragg-Brentano geometry using a D8-Advance instrument (Bruker AXS). Fig. 1 shows the diffraction pattern measured with Cu Kα radiation (λ = 0.154 nm). The positions of the diffraction lines according to the powder diffraction database (PDF) with (*h k l*) = (1 1 1), (2 0 0), (2 2 0), (3 1 1) and (2 2 2) are indicated for 3C–SiC (PDF 29-1129) and graphite with (*h k l*) = (0 0 2) (PDF 41-1487). Non-indicated lines are formed by the sintering additive $YAlO_3$ (PDF 38-0222).

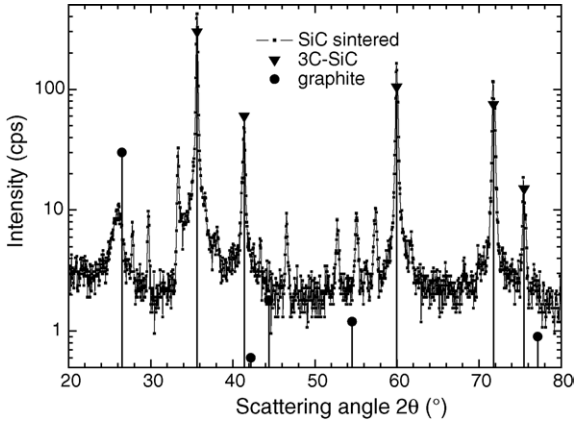

Fig. 1. Normalized scattering intensity from XRD of the SiC/SiC composite sample as a function of scattering angle 2*θ* measured with Cu Kα radiation (λ = 0.154 nm). The (1 1 1), (2 0 0), (2 2 0), (3 1 1) and (2 2 2) peaks of 3C–SiC as well as the (0 0 2) peak of graphite are indicated.

XRD clearly shows the existence of the 3C–SiC polytype, and no indication of another SiC polytype is observed. The cubic polytype has the highest symmetry and, therefore, shows the lowest number of diffraction lines. All lower symmetric SiC polytypes give diffraction lines near to and between the positions of the 3C–SiC diffraction lines. However, no intensity is found at the "between position", e.g. at $2\theta = 34.2^\circ$, 38.2°, 65.8° and 73.6° for 6H–SiC. The diameter of the SiC crystallites is ~60 nm, as calculated from the line width after deconvolution of the measured data with the instrumental resolution. This indicates the size of regions showing coherent scattering. As this value is about twice the diameter of the nano-particles availed for sintering, this is another indication of the perfectness of the sintered body. In particular, no real grain boundaries are indicated but just a disturbance of translational symmetry in one crystal direction (here, the surface normal of the 10 mm × 10 mm sample face), whereas the other crystal directions may keep translational symmetry. Furthermore, only the most intense graphite line (0 0 2) was measured because other lines have a more than one order less intensity in randomly oriented graphite: the intensity of the next intense (1 0 1) line is only 6% of the intensity of the (0 0 2) line.

3.2. Atomic force microscopy

The surface morphology of the SiC/SiC sample was investigated by AFM using a closed-loop scanner, which allows high precision measurements on the nanometer scale. All measurements were recorded under ambient conditions in 'Tapping Mode' [14,15]. Silicon-tips with a typical tip radius smaller than 10 nm and an opening angle of less than 20° were applied. The scanner's large measurement range of 15 μm in the vertical direction was in particular beneficial for this investigation since the sample exhibits – due to the manufacturing process – a significant root mean square (RMS) roughness of RMS ~ 300 nm and maximum height differences of about 1.5 μm on a 10 μm × 10 μm image.

The AFM results are summarized in Fig. 2 showing representative images ranging from 10 μm × 10 μm to 1 μm × 1 μm scan size. The large area scan (Fig. 2a) leaves the overall impression that the surface is characterized by two main morphological features:

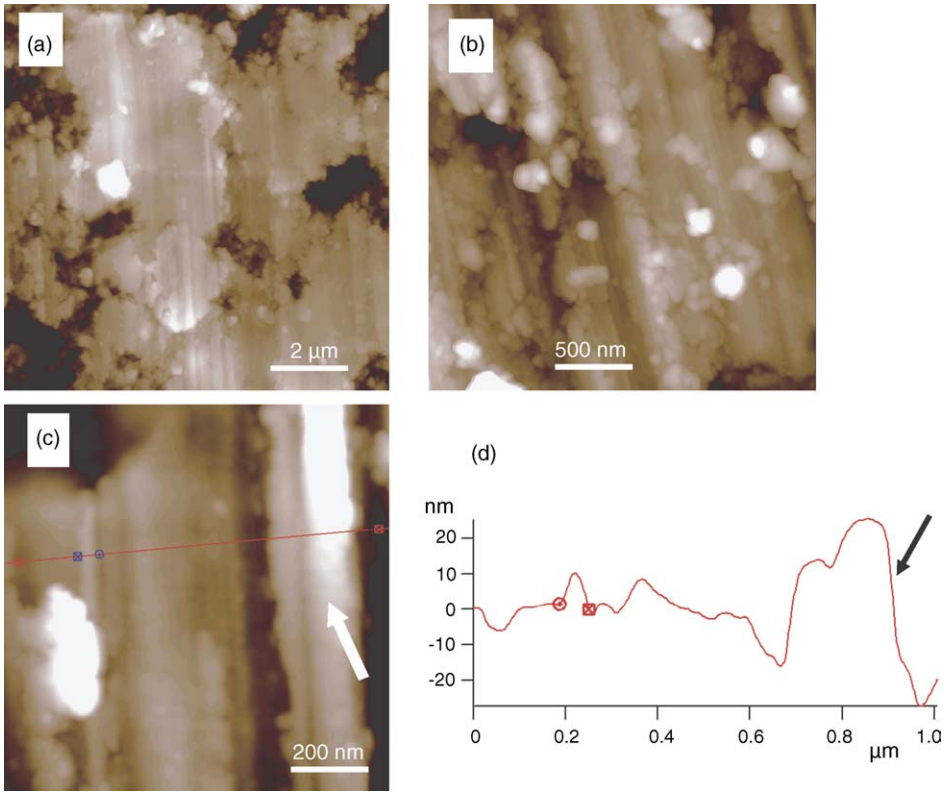

Fig. 2. AFM images of the SiC/SiC composite sample. (a) 10 μm × 10 μm image representing the overall sample morphology. The grey scale range is 500 nm. (b) 2.5 μm × 2.5 μm AFM image of a different sample position. The grey scale range is 200 nm. The 3D crystallites are either arranged along the furrows on a fibre ply, or are irregularly distributed on the surface. (c) 1 μm × 1 μm AFM image showing a small fraction of a fibre ply in the left part of the image. The arrow indicates a larger ridge with a step. The grey scale range is 50 nm. (d) Section analysis along the line indicated in (c).

first, small three-dimensional (3D) crystallites and second, unidirectional oriented elongated structures. The latter can clearly be addressed to the SiC fibres of the composite sample. Whereas individual isolated fibres are rarely observed, a large fraction of them occurs in densely packed two-dimensional (2D) arrays. It seems that such 2D-ply fibres are embedded in the matrix of 3D crystallites. One ply usually extends over an area of about 5 μm × 5 μm (Fig. 2a) with frayed edges. From the line section presented in Fig. 2d, we can assume that the fibres have a circular cross-section. Their diameters range between 40 and 55 nm.

The 3D crystallites have an average diameter of about 50 nm ranging from 25 to almost 100 nm. This finding is in excellent agreement with the results from XRD discussed above. Within certain areas the crystallites are rather uniform. Small crystallites sized 30 ± 5 nm in diameter can be found in irregular arrays over a few percent of the surface. Larger crystallites with 75 ± 15 nm diameter, occupying about 15% of the area of the surface, are frequently observed along the furrows between the fibres (Fig. 2b). Due to the overall roughness of the sample it was impossible to reveal the 3D shape (facets) of the crystallites.

In addition to the crystallites and fibre plies, larger ridges are occasionally observed—indicated by arrows in Fig. 2c and d. These ridges have a lateral size of about 250 nm and are on average 50 nm high. The line section in Fig. 2d reveals a second step on top of the larger ridge, which is about 12 nm high. The nature of these features is not yet clear.

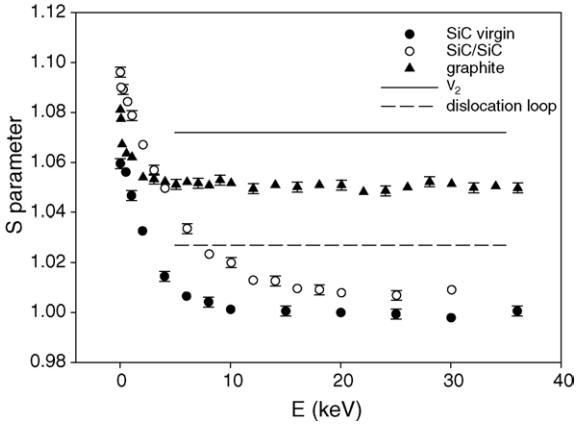

Fig. 3. Lineshape parameter S for different silicon carbide samples and pyrolytic graphite as a function of incident positron energy E. For comparison, the S values of dislocation loops and Si + C divacancies (V_2) in 6H–SiC are given.

3.3. Slow positron implantation spectroscopy

SPIS results of the SiC/SiC sample are presented in Fig. 3. For comparison, SPIS data from a very clean pyrolytic graphite sample (of unknown origin) and crystalline 6H–SiC (provided by CREE Research Inc., Durham, NC, USA; (0 0 0 1)-oriented (3.5° off), Si-faced, n-type) are given.

A positron diffusion length of $L_+ = 186 \pm 6$ nm is calculated for the composite, which needs to be compared to the values of epi-6H–SiC ($L_+ = 157 \pm 36$ nm) and crystalline 6H–SiC ($L_+ = 54 \pm 3$ nm), respectively [12]. This comparison already suggests that the composite has the lowest defect concentration. However, it seems to be a contradiction that at higher positron implantation energies the bulk value of the composite is found to be slightly above the bulk value of the 6H–SiC sample. On the other hand, from previous positron lifetime calculations [16] it became clear that differences in the structure of the SiC polytypes 3C, 4H and 6H are below the detection limit of ordinary PAS, and thus the same bulk value for 3C and 6H has to be expected. Therefore, a most natural explanation of the results from Fig. 3 is that positron annihilation is occurring partly in graphite, which is definitely still contained in the composite sample according to XRD results.

From the results shown in Fig. 3, a positron diffusion length of $L_+ = 42 \pm 9$ nm is calculated for the pyrolytic graphite. Supposing that there is no preferential positron annihilation in graphite compared to 3C–SiC, a linear dependency may be assumed:

$$S_{\text{composite}} = (1 - m)S_{\text{3C-SiC}} + mS_{\text{graphite}} \quad (1)$$

From the comparison of bulk S values shown in Fig. 2a it is found that $m = 0.16 \pm 0.04$. Then, a similar assumption can be made regarding the measured positron diffusion length L_+ of the composite provided the two phases form parallel channels to the surface:

$$L_{\text{composite}} = (1 - m)L_{\text{3C-SiC}} + mL_{\text{graphite}} \quad (2)$$

Inserting all numbers, one obtains a 'true' value of $L_+ \sim 213$ nm for 3C–SiC. This remarkably large number indicates that defect-free grains should have a diameter of at least twice this value, i.e. ~426 nm, but most probably are formed much larger in size by the sintering process. Indeed, this may be the case as the fibres and some particles have a size similar to the estimated effective diffusion length. Thus, grain boundaries, which might perhaps act as trapping sites for positrons too, are evenly distributed through the macroscopic sample made up of defect-free grains and do not play any significant role.

Although dislocation loops and Si + C divacancies (V_2) have S values above the bulk value of 6H–SiC and the composite (see Fig. 3), they are unlikely to exist in the composite due to its preparation from 3C–SiC nano-crystalline material at high temperature conditions. To judge whether they exist or not, one option is an improved approach for the analysis of SPIS Doppler broadening data introduced by using a combination of Doppler broadening lineshape parameters S and W [17,18]. These results are shown in Fig. 4.

Any material state, like the bulk or a certain defect, is characterized by a given set of lineshape parameters, i.e. (S, W) values, which are required to be deduced in the same way from experimental data. In case of silicon carbide, from previous work (see ref. [9] and references therein) it became possible to include in Fig. 4 the (S, W) values for dislocation loops and the V_2 defect, both being of 'open volume type' although to different extents. When only two distinct annihilation characteristics, described by (S_1, W_1) and (S_2, W_2), contribute to a set of experimental data, a

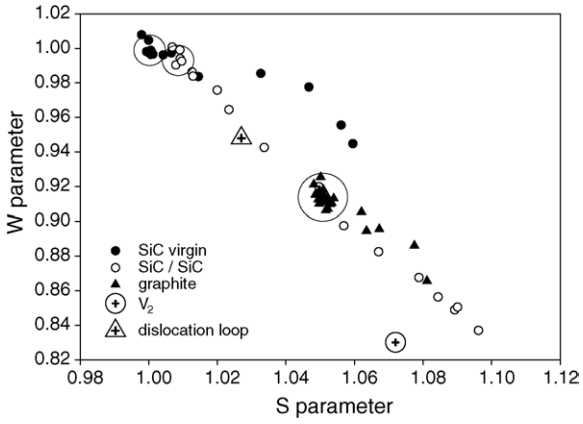

Fig. 4. Normalized lineshape parameters W/W_b vs. S/S_b plot for different silicon carbide samples, defect states in 6H–SiC and pyrolytic graphite. An untreated Si(1 0 0) sample served as a reference (S_b, W_b) for normalization.

straight line is obtained in the S–W representation where the endpoints represent the two states itself [17,18]. If (S_1, W_1) is taken to represent the 6H–SiC bulk, and (S_2, W_2) to represent the V_2 defect, then a straight line connecting both states should contain the (S, W) values of all defects having an open volume less than the V_2 defect. Indeed, the (S, W) value representing dislocation loops is found to be located correctly regarding its W value but shifted slightly in S towards the value of bulk pyrolytic graphite (see Fig. 3). This could be an indication that in the dilatation part of the dislocation loops observed in Al^+ implanted 6H–SiC (see ref. [9] and references therein) the positron annihilates preferentially at carbon atoms. From Al^+ implantation into 4H–SiC [19], it was concluded that excess Si interstitials, being generated in a substitutional process upon annealing, form the dislocation loops. For the composite, the bulk W value is negligibly different from the corresponding value for 6H–SiC, which is an indication that trapping at grain boundaries can be neglected. However, the noticeable shift in S towards the graphite value is a direct confirmation of positron annihilation in graphite still contained in the composite.

The SPIS results are another indication of the perfectness of the composite in agreement with the findings from XRD described above, and furthermore a very nice confirmation of a perfectly sintered body already found by TEM [13]. Now the TEM results are confirmed at atomic level by PAS because any possible remaining open volume fraction should be at a lower than in the crystalline 6H–SiC sample.

3.4. Positron affinity

The positron affinity A_+ as a bulk quantity is defined by [20]:

$$A_+ = \mu_- + \mu_+ = -(\Phi_- + \Phi_+). \quad (3)$$

Here, Φ_+ and Φ_- are the positron and electron work functions, and μ_- and μ_+ are the electron and positron chemical potentials, respectively. First-principles electronic structure and positron-state calculations for perfect and defected 3C–SiC and 6H–SiC were already calculated by assuming that μ_- corresponds to the top of the valence band [5]. On the other hand, when comparing positron affinities of two materials in contact (SiC and graphite here), one should be aware of actual position of electron chemical potentials (Fermi levels) of both materials (cf. [21]). Nevertheless, we adopt here the same approach as in [5] because the actual position of the Fermi level in the SiC composite is unknown. However, this simplification does not influence conclusions given below.

The positron affinity is a very useful materials property to judge whether positrons become trapped by precipitates. This concept implies an even distribution of precipitates in a host matrix. Then, a positron will be trapped by a spherical precipitate if the difference ΔA_+ between the positron affinity of the host and the precipitate is positive and the radius of the precipitate exceeds a critical radius r_c given by [20]:

$$r_c = \frac{0.31}{(\Delta A_+)^{1/2}} \quad (4)$$

The proportionality constant has the dimension $nm(eV)^{1/2}$, ΔA_+ is given in eV and r_c is given in nm. This 'positron affinity concept' was successfully applied to consider, e.g. irradiation-induced precipitates in reactor pressure vessel steels [22], and clustering of Ge [16] and B [23] in 6H–SiC due to ion implantation and annealing.

Here, the positron affinity of graphite is of interest. The application of different calculational methods has been described already in detail elsewhere [5]. Here, we mention that we employ the linear-muffin-tin-orbital

Table 1
Positron lifetimes (τ) and affinities (A_+) for graphite calculated using different computational methods and approaches (see text) to electron–positron correlations

Theory	LMTO		ATSUP
	τ (ps)	A_+ (eV)	τ (ps)
BN	174	−9.0	185
GC	186	−8.3	206

(LMTO) method [24]. In the framework of this method, one often needs to incorporate empty spheres (ES) into the studied structure in order to describe properly the (electron and positron) charge distribution in the interstitial space [24]. We tried several choices of the ES sizes and positions and the results presented in Table 1 correspond to the most realistic case. Boronski–Nieminen (BN) scheme [25] and gradient correction (GC) approach of Barbiellini et al. [26] were employed to treat electron–positron correlation effects.

The positron affinity of graphite is found to be positioned well below the one of 3C–SiC ($A_+ = -5.57$ eV [5]) independent of the various potentials chosen in the particular calculations and also independent of the position of the 3C–SiC Fermi level. This indicates that graphite precipitates (or 'regions') imbedded in a 3C–SiC host matrix would be attractive to positrons. A formal application of Eq. (4) and inserting numbers from Table 1 would give a critical radius of the order $r_c \sim 0.1674$–0.1876 nm. The lattice parameters of graphite can be found from XRD (PDF 41-1487) thus giving the lattice constants $a = 0.24704$ nm and $c = 0.67244$ nm. Because carbon atoms may touch each other at the utmost within the (0 0 0 1) face, the 'atomic radius' of a carbon atom should be less equal $a/2$, i.e. 0.1235 nm. Taking this number, another formal calculation gives the result that a 'graphite precipitate' able to trap a positron inside a 3C–SiC matrix should contain at least three to four carbon atoms. Certainly, such a consideration is not applicable to the given composite sample because the carbon is not evenly distributed inside the 3C–SiC matrix. From the production process described above, it is more probable to have maybe continuous carbon threads after the sintering process. Anyway, the attractiveness of graphite overestimates the carbon ratio m in Eqs. (1) and (2), i.e. the assumed linear dependency does not really exist. Nevertheless, the estimated order of the positron diffusion length in 3C–SiC should remain correct.

3.5. Positron lifetime

In addition to the positron affinity, the positron lifetime is also calculated, and both the LMTO and atomic superposition (ATSUP) [27,28] methods are used for this purpose (see Table 1). The lifetime results obtained using these two methods differ non-negligibly. This is probably due to LMTO limitations to describe properly the interstitial space. The ATSUP-BN results compare well with other calculated lifetimes presented in the literature [29,30], on the other hand, our ATSUP-GC value agrees well with 209 ps given [31] and obtained using a different approach.

Positron lifetime measurements on the pyrolytic graphite and SiC/SiC composite samples were performed using a spectrometer of 160 ps time resolution (FWHM at ^{22}Na window settings) which is described in detail elsewhere [32]. The measured positron lifetime spectrum of graphite was decomposed into two components: $\tau_1 = 93 \pm 4$ ps and $\tau_2 = 242 \pm 4$ ps with corresponding intensities $I_1 = 23 \pm 1\%$ and $I_2 = 77 \pm 1\%$. The components τ_1 and τ_2 are attributed to delocalized and trapped positrons, respectively. When the two state trapping model is considered, the corresponding bulk positron lifetime amounts to $\tau_b = 177 \pm 1$ ps, which corresponds reasonably well to the calculated lifetimes given in Table 1, the LMTO-BN number being the closest one. Measured positron lifetimes presented in literature (see [29–31] and references therein) range from 195 to 215 ps but were measured with time resolutions being worse than the presently used. From the above two components, we also calculated the mean positron lifetime $\tau_{av} = 208 \pm 3$ ps that falls into this range. This indicates that a lifetime of about 200 ps usually measured in graphite corresponds to a mixture of delocalized and localized positrons. However, the nature of positron trapping sites is not fully certain, these could be monovacancies and/or small vacancy clusters on the basis of calculations given in [31].

As for the SiC/SiC composite sample, we decided to fix one of lifetime components to τ_{av} for graphite – as given above – because our sample contains graphite 'regions' (as indicated by SPIS measurements) which

re attractive to positrons—as follows from positron affinity results. Then, the fitting procedure results in three components $\tau_1 = 141 \pm 6$ ps, $\tau_2 = 208$ ps and $\tau_3 = 320 \pm 6$ ps with the following intensities: $I_1 = 65 \pm 9\%$, $I_2 = 15 \pm 7\%$ and $I_3 = 20 \pm 7\%$. This further confirms the presence of graphite in the SiC/SiC composite sample though the corresponding annihilation fraction calculated from lifetime results (considering the three state trapping model) amounts to 5% only, which is somewhat less than 16% obtained from SPIS data (based on an assumed linear dependency of change in S values). Considering further the trapping model, the bulk lifetime calculated is 168 ps, which is somewhat too high compared to the experimental bulk lifetime of 3C–SiC (138 ps [16]). These findings indicate that our interpretation of the lifetime measurement is not perfect, but at this moment we do not have enough knowledge about the studied sample to suggest a better one.

3.6. Re-emission of positrons

The persistence of positron re-emission from a sample up to positron implantation energies of several kiloelectron volts is characteristic of work-function emission [34]. Thus, an estimation of Φ_+ from re-emission measurements relies on the fact of Φ_+ being a negative quantity and has been successfully applied to determine Φ_+ for 6H–SiC [6]. However, in case of Φ_+ being a positive quantity another experimental method employing positrons was already published [33].

Results of positron re-emission measurements at the SiC/SiC sample in comparison with a crystalline 6H–SiC sample are presented in Fig. 5. For the composite, the dependence of re-emitted positron yield (the fraction of incident positrons re-emitted at low energies) on incident positron energy E is characteristic of epithermal positron emission, becoming significant only at incident energies below 1 keV with a fitted effective positron diffusion length of $\leq$1 nm. Because the re-emitted positron fraction is measurably non-zero above 1 keV, in conflict with the epithermal emission model used to fit the data, it is possible that for the composite there is a very small, long 'tail' of work-function re-emission extending to several kiloelectron volts; the line on the graph

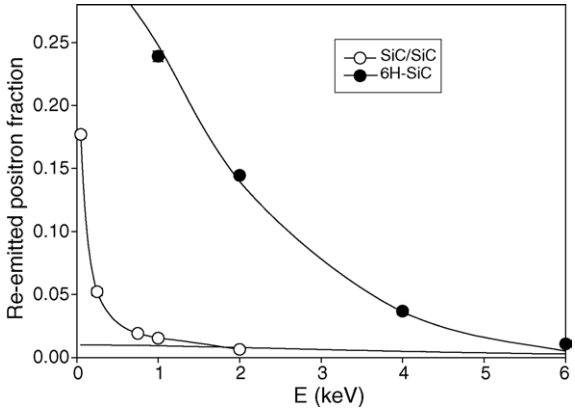

Fig. 5. Re-emitted positron yields from the SiC/SiC composite and a crystalline 6H–SiC sample. Solid lines are fits using diffusion lengths of 45 nm (6H–SiC) and 1 nm (epithermal) and 200 nm (thermal positrons) (composite).

corresponds to a positron diffusion length of $L_+ = 200$ nm (as suggested by the S parameter measurements of Fig. 3) and a zero-energy yield of 0.01—about 30 times smaller than the same yield for 6H–SiC. In comparison, a piece of 6H–SiC shows typical work-function re-emission, albeit in this case with a rather small diffusion length of $L_+ \sim 45$ nm. The data are thus consistent with the picture of a very low branching ratio for work-function re-emission from the composite. It could be that any work-function re-emission that does occur is from the small ($\sim$30 nm diameter) crystallites seen by AFM, as described in Section 3.2, and that the surface fibres – perhaps coated with graphite – and the larger crystallites (which are buried in surface furrows) do not re-emit thermalized positrons efficiently.

Re-emitted positron spectra of the SiC/SiC sample in comparison with a crystalline 6H–SiC sample are presented in Fig. 6. These data were taken for both samples by measuring annihilation gamma count rates from the samples as a stopping potential was ramped from 2 to -5 V. As the potential becomes increasingly negative, more re-emitted positrons are returned to the sample and are annihilated there. Only annihilation events in the sample are observed; a thick lead slit is placed between the sample and detector. To obtain acceptable counting statistics, the sintered SiC data were taken for an incident positron energy of 0.5 keV. The shapes of the two spectra are essentially the same,

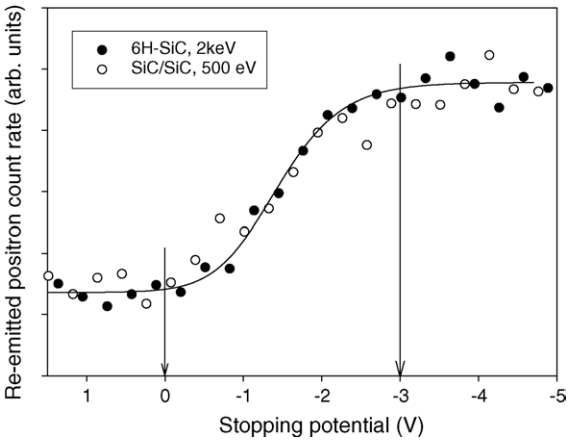

Fig. 6. Re-emitted positron spectra from the SiC/SiC composite and a crystalline 6H–SiC sample as a function of stopping potential. Solid line: fit to the data. The two arrows indicate zero and maximum positron energies, yielding a value for the positron work function = 3.0 ± 0.3 eV.

to within statistical uncertainty. This supports the view that there may be low-level work-function re-emission from the sintered sample at 0.5 keV. However, the unavoidable experimental scatter in the data may obscure a small epithermal tail to higher energies (on the right of the plot). The work function suggested by these measurements is $\Phi_+ = 3.0 \pm 0.3$ eV, close to the previously measured values [6].

SPIS data of the SiC/SiC sample and a 6H–SiC sample, taken just for comparison at the Bath, UK positron beamline, give diffusion lengths of 186 and 45 nm for the composite and crystalline samples, respectively, when analysed by VEPFIT. These diffusion lengths are consistent with the curves drawn on Fig. 5 for work-function re-emission, although for the composite sample epithermal re-emission dominates at low energies. The bulk S value is found to be higher for the SiC/SiC sample, in agreement with results presented in Fig. 3.

In summary, the positron re-emission measurements (Figs. 5 and 6) – in combination with comparative SPIS studies – suggest that, although the diffusion length for thermalized positrons in the composite is rather long, the probability for positron re-emission by the 3 eV work function is very small—at most 3% of that for a single-crystal 6H–SiC sample.

4. Conclusions

It has been experimentally demonstrated by XRD that a macroscopic SiC/SiC composite sintered from nano-crystalline 3C–SiC consists exclusively of 3C–SiC containing still some graphite inclusions.

AFM measurements on different areas of the composite sample reveal that micrometer sized 2D plies of SiC fibres are embedded in a matrix of 3D crystallites with diameters in the range between 30 and 90 nm.

SPIS investigations underline the perfectness of the composite at an atomic size level due to the sintering process used, and demonstrate that depth profiling of defects is not hindered by a large surface roughness.

From positron affinity calculations it becomes clear that graphite embedded in 3C–SiC is attractive to positrons.

Positron lifetime measurements indicate also the presence of graphite in the SiC/SiC composite studied.

Appreciable re-emission from the SiC/SiC sample is only observed for incident positron energies below 1 keV, characteristic of epithermal positron emission.

Acknowledgement

The authors express their gratitude to Dr. V. Heera (FZ Rossendorf) for valuable discussions of various aspects of this work.

References

[1] L.L. Snead, R.H. Jones, P. Fenici, A. Kohyama, J. Nucl. Mater. 233–237 (1996) 26.
[2] Advanced SiC/SiC ceramic composites: developments and applications in energy systems, in: A. Kohyama, M. Singh, H.-T. Lin, Y. Katoh (Eds.), Ceramic Transactions, vol. 144, American Ceramic Society, Westerville, OH, 2002.
[3] V. Heine, C. Cheng, R. Needs, J. Am. Ceram. Soc. 74 (1991) 2630.
[4] M.J. Rutter, V. Heine, J. Phys.: Condens. Matter 9 (1997) 8213.
[5] G. Brauer, W. Anwand, E.-M. Nicht, J. Kuriplach, M. Sob, N. Wagner, P.G. Coleman, M.J. Puska, T. Korhonen, Phys. Rev. B 54 (1996) 2512.
[6] J. Störmer, A. Goodyear, W. Anwand, G. Brauer, P.G. Coleman, W. Triftshäuser, J. Phys.: Condens. Matter 8 (1996) L89.

[7] Silicon carbide and related materials 2004, in: R. Nipoti, A. Poggi, A. Scorzoni (Eds.), Mater. Sci. Forum, vol. 483–485, Trans Tech Publications, Uetikon-Zürich, 2005.
[8] R. Krause-Rehberg, H. Leipner, Positrons in Semiconductors—Defect Studies, Springer, Heidelberg, 1999.
[9] G. Brauer, W. Anwand, P.G. Coleman, W. Skorupa, Vacuum 78 (2005) 131.
[10] G. Binnig, K.F. Quate, C. Gerber, Phys. Rev. Lett. 56 (1986) 930.
[11] C. Teichert, Phys. Rep. 365 (2002) 335.
[12] G. Brauer, W. Anwand, W. Skorupa, S. Brandstetter, C. Teichert, J. Appl. Phys., submitted for publication.
[13] Y. Katoh, S. Dong, A. Kohyama, in [2], p. 77.
[14] Q. Zhong, D. Inniss, K. Kjoller, V.B. Elings, Surf. Sci. 290 (1993) L688.
[15] E. Meyer, H.J. Hug, R. Bennewitz, Scanning Probe Microscopy: The Lab on a Tip, Springer, Berlin, 2004.
[16] G. Brauer, W. Anwand, P.G. Coleman, A.P. Knights, F. Plazaola, Y. Pacaud, W. Skorupa, J. Störmer, P. Willutzki, Phys. Rev. B 54 (1996) 3084.
[17] M. Clement, J.M.M. De Nijs, A. van Veen, H. Schut, P. Balk, J. Appl. Phys. 79 (1996) 9029.
[18] M. Clement, J.M.M. De Nijs, A. Van Veen, H. Schut, P. Balk, IEEE Trans. Nucl. Sci. 42 (1995) 1717.
[19] P.O.A. Persson, L. Hultman, M.S. Janson, A. Hallen, R. Yakimova, J. Appl. Phys. 93 (2003) 9395.
[20] M.J. Puska, P. Lanki, R.M. Nieminen, J. Phys.: Condens. Matter 1 (1989) 6081.
[21] G. Brauer, W. Anwand, W. Skorupa, A.G. Revesz, J. Kuriplach, Phys. Rev. B 66 (2002) 195331.
[22] G. Brauer, M.J. Puska, M. Sob, T. Korhonen, Nucl. Eng. Des. 158 (1995) 149.
[23] W. Anwand, G. Brauer, J. Kuriplach, W. Skorupa, Mater. Sci. Forum 445–446 (2004) 36.
[24] For a recent review, see O.K. Andersen, O. Jepsen, M. Sob, in: M. Yussouff (Ed.), Electronic Band Structure and Its Applications, Springer, Berlin, 1987, p. 1.
[25] E. Boronski, R.M. Nieminen, Phys. Rev. B 34 (1986) 3820.
[26] B. Barbiellini, M.J. Puska, T. Torsti, R.M. Nieminen, Phys. Rev. B 51 (1995) 7341.
[27] M.J. Puska, R.M. Nieminen, J. Phys. F: Met. Phys. 13 (1983) 333.
[28] A.P. Seitsonen, M.J. Puska, R.M. Nieminen, Phys. Rev. B 51 (1995) 14057.
[29] M.J. Puska, R.M. Nieminen, J. Phys.: Condens. Matter 4 (1992) L149.
[30] S. Ishibashi, J. Phys.: Condens. Matter 14 (2002) 9753.
[31] Z. Tang, M. Hasegawa, T. Shimamura, Y. Nagai, T. Chiba, Y. Kawazoe, M. Takenaka, E. Kuramoto, T. Iwata, Phys. Rev. Lett. 82 (1999) 2532.
[32] F. Becvar, J. Cizek, L. Lestak, I. Novotny, I. Prochazka, F. Sebesta, Nucl. Instrum. Meth. A 443 (2000) 557.
[33] A.P. Mills Jr., P.M. Platzman, B.L. Brown, Phys. Rev. Lett. 41 (1978) 1076.
[34] A.H. Weiss, S. Yang, H.Q. Zhou, E. Jung, A.R. Koymen, S. Naidu, G. Brauer, M.J. Puska, Appl. Surf. Sci. 85 (1995) 82.